2005

Analysis, representation, and prediction of creep transients in Class I alloys

Taleff, Eric M.; Green, W. Paul; Kulas, Mary-Anne; McNelley, Terry R.; Krajewski, Paul E.

Elsevier

E.M. Taleff, W.P. Green, M.-A. Kulas, T.R. McNelley, P.E. Krajewski, "Analysis, representation, and prediction of creep transients in Class I alloys," Materials Science & Engineering A, v. 410-411, (2005) pp. 32-37
http://hdl.handle.net/10945/55868

Materials Science and Engineering A 410–411 (2005) 32–37

www.elsevier.com/locate/msea

Analysis, representation, and prediction of creep transients in Class I alloys

Eric M. Taleff [a,*], W. Paul Green [a], Mary-Anne Kulas [a], Terry R. McNelley [b], Paul E. Krajewski [c]

[a] *The University of Texas at Austin, Department of Mechanical Engineering, 1 University Station, C2200 Austin, TX 78712-0292, USA*
[b] *Naval Postgraduate School, Department of Mechanical Engineering, 700 Dyer Road, Monterey, CA 93943-5146, USA*
[c] *General Motors Corp., Research and Development Center, 30500 Mound Road, Warren, MI 48090-9056, USA*

Received in revised form 4 April 2005

Abstract

Solute-drag (SD) creep in Class I alloys is characterized by several features. Among these is the presence of "inverse" creep transients, which are unique to these solid-solution alloys and the SD creep mechanism. Creep transients in commercial AA5083 materials under SD creep are analyzed using a model based on a graphical construct previously proposed. It is observed that transient behavior can be represented in a general fashion which predicts the decay in relative transient size as a function of strain. Experimental data for SD creep are presented using the proposed graphical construct to determine the dependence of dislocation glide speed on stress and the dependence of equilibrium mobile dislocation density on stress. It is observed that the high stress exponents of the commercial AA5083 materials under SD creep, relative to low-impurity, binary Al–Mg materials, are primarily the result of an increased dependence of dislocation glide speed on stress.

Keywords: Creep; Solute-drag creep; Creep transients; Dislocation density; Al–Mg

1. Introduction

Solute-drag (SD) creep is an important mechanism of deformation in Al–Mg alloys, including 5000-series commercial Al alloys, at elevated temperature and slow strain rate [1–25]. Alloys which exhibit SD creep are referred to as either Class I [2] or Class A [5] alloys. SD creep is characterized by a stress exponent, n, of approximately three and an activation energy for creep, Q_c, close to that of solute diffusion when observed in low-impurity, binary alloys. SD creep is insensitive to grain size [26], although grain-boundary-sliding (GBS) creep will supplant SD creep when grain size is fine [23]. In low-impurity, ternary Al–Mg–Mn alloys and commercial 5000-series alloys, the stress exponent can exhibit values up to approximately four [22–25]. In all these alloy types, SD creep is characterized by creep transients of the "inverse" type [27]. The term *inverse* is used because these transients are opposite those displayed by pure metals and Class II (Class M) alloys [2,5]. Strain-rate-change (SRC) tests, in which a series of constant strain rates are imposed on a specimen, can be used to study transient behavior by recording flow stress response immediately following rate changes. In such tests, the inverse transients characterizing SD creep are evidenced as follows. For an increase in strain rate, the flow stress undergoes a large, abrupt increase and then decays toward a steady-state value at the new, increased strain rate. Upon a decrease in strain rate, flow stress undergoes a large, abrupt decrease and then gradually increases to a steady-state value at the new, reduced strain rate. Such inverse transients are exhibited only by SD creep and, as such, have been used to positively identify the presence of this deformation mechanism [25].

Quick plastic forming (QPF), a process related to superplastic forming, utilizes AA5083 sheet material to mass produce automobile body panels [28]. Fine-grained, commercial, superplastic AA5083 materials demonstrate creep deformation by either GBS or SD creep across conditions typical of QPF operations [25]. Although GBS creep is typically associated with superplastic deformation, primarily because of the low stress exponent of $n \approx 2$ which it provides, the slightly higher stress exponents of SD creep, $n = 3$–4, in commercial 5000-series alloys can also provide significantly enhanced tensile ductility [29]. The QPF

* Corresponding author. Tel.: +1 512 471 5378; fax: +1 512 471 7681.
E-mail address: taleff@mail.utexas.edu (E.M. Tsaleff).

0921-5093/$ – see front matter © 2005 Elsevier B.V. All rights reserved.
doi:10.1016/j.msea.2005.08.085

Table 1
Sheet thickness, t, and composition of each AA5083 material

Material	t (mm)	Composition (wt.%)						
		Si	Fe	Cu	Mn	Mg	Cr	Al
DC-C	1.2	0.15	0.20	0.03	0.76	4.50	0.07	Balance
CC-A	1.0	0.07	0.22	0.02	0.72	4.70	–	Balance

process takes advantage of this effect of SD creep to form at faster rates and lower temperatures than traditionally used for superplastic forming. Because the creep transients which occur under SD creep are significant in size and duration, it is important that these transient behaviors be correctly predicted in order to model the QPF process. Unfortunately, a general means of modeling creep transients under SD creep does not yet exist. The purpose of the present investigation is to create a means of quantitatively predicting transient behaviors by analyzing experimental data for SD creep in AA5083 sheet materials.

2. Materials

Two commercial AA5083 sheet materials are considered for this investigation. One is a direct-chill-cast product, material DC-C, and one is a continuously cast product, material CC-A. Both materials were produced in sheet form by cold rolling to an approximately H18 temper. The compositions of these materials, which are very similar, have been previously reported and are summarized in Table 1 [25]. Studies of these materials at 450 °C have shown them to deform by SD creep at fast strain rates ($\dot{\epsilon} \geq 10^{-3}\,\mathrm{s}^{-1}$) and by GBS creep at slow strain rates ($\dot{\epsilon} < 10^{-3}\,\mathrm{s}^{-1}$) [25]. Samples of each material were subjected to tensile SRC tests at 450 °C using a series of constant engineering strain rates within the SD creep regime. A variety of strain-rate changes were used to produce creep transients. The details of these experiments and some of the resulting transient data have been previously reported [25]. The steady-state behavior and size of transients were evaluated [25]. The present investigation addresses details of the rate of decay in stress transients with strain not previously considered.

3. Transient behaviors

The majority of creep analyses focus on "steady-state" behavior. Analysis of steady-state data is often conducted using the phenomenological equation for creep [30–34]:

$$\dot{\epsilon} = A\left(\frac{b}{d}\right)^{p}\left(\frac{\sigma}{E}\right)^{n}\exp\left(-\frac{Q_c}{RT}\right), \tag{1}$$

where $\dot{\epsilon}$ is the true-strain rate, A a constant which depends on the material and the dominant deformation mechanism, b the magnitude of the Burgers vector, d the grain size, p the grain-size exponent, σ the true flow stress, E the unrelaxed temperature-dependent elastic modulus, n the stress exponent, Q_c the activation energy for creep, R the universal gas constant, and T is the absolute temperature. However, non-steady creep behaviors hold a wealth of information which can often better reveal the fundamental mechanisms of creep deformation. Recent examples of exploiting non-steady data from full creep curves using the θ-projection method [35,36] are found in the work of Wilshire and colleagues [37,38]. In hot forming applications using AA5083 materials, such as QPF, loading conditions are also non-steady and, thus, are quite different from those of the creep tests to which the θ-projection method is typically applied. Prediction of transient behaviors for these processes, therefore, requires a slightly different approach. Non-steady loadings can lead to significant creep transients during forming operations when SD creep governs deformation, making the prediction of transient behaviors of practical significance. Previous investigations have studied the magnitudes of creep transients under SD creep, but have not explained the decay of transients with strain [12,13,25].

In order to analyze the creep transients produced under SD creep, some understanding of the SD creep mechanism is required. SD creep has been extensively studied in low-impurity, binary alloys, such as Al–Mg [1–21]. These studies reveal the stress exponent to be $n = 3$ and an activation energy for creep equal to the activation energy for solute diffusion, $Q_c = Q_{sol}$. The most-accepted model of SD creep, proposed by Weertman [39–41], predicts these observed relationships and can be summarized as follows. The rate of creep deformation is controlled by glide of dislocations under the influence of a dragging solute atmosphere. Because subgrains do not generally form under SD creep, i.e. any structures which could be considered as subgrains are quite loose and ill organized, and dislocations are generally well distributed, the Orowan relation is accepted as applicable under SD creep. The Orowan relation is

$$\dot{\gamma} = \rho b \bar{v}, \tag{2}$$

where $\dot{\gamma}$ is shear strain rate, ρ the density of mobile dislocations, and $\bar{v}$ is the average rate of dislocation glide under solute drag. The mobile dislocation density is estimated using the Taylor relation, $\rho \propto \tau^2$, which is supported by dislocation-density measurements from Horiuchi and Otsuka [3]. Various models for dislocation motion under solute drag predict that dislocation glide speed is directly proportional to applied stress and solute diffusivity, $\bar{v} \propto D_{sol}\tau$ [42–47]. The Weertman model, thus, predicts the observed values of stress exponent and creep activation energy. However, the "constant-structure" data of Mills et al. contradict the stress dependencies of ρ and $\bar{v}$ predicted by this model. Their data indicate that $\rho \propto \tau$, contrary to the model assumption and measurements from Horiuchi and Otsuka [3], and $\bar{v} \propto \tau^2$ under SD creep [12]. Thus, while the SD creep model predicts the observed steady-state behaviors, it is inconsistent with the observed non-steady behaviors. The SD creep model also fails to predict the observed behaviors of more complex Al–Mg-based alloys, such as ternary Al–Mg–Mn alloys and commercial 5000-series alloys, which clearly deform by SD creep but exhibit n values greater than three [22–25,29]. The present investigation uses new experimental data to further clarify these cases.

SRC test data, from a transient-behavior test, for material DC-C are presented in Fig. 1. These data clearly show inverse transients following abrupt rate changes. Stress transients following rate changes are found to obey the following relation

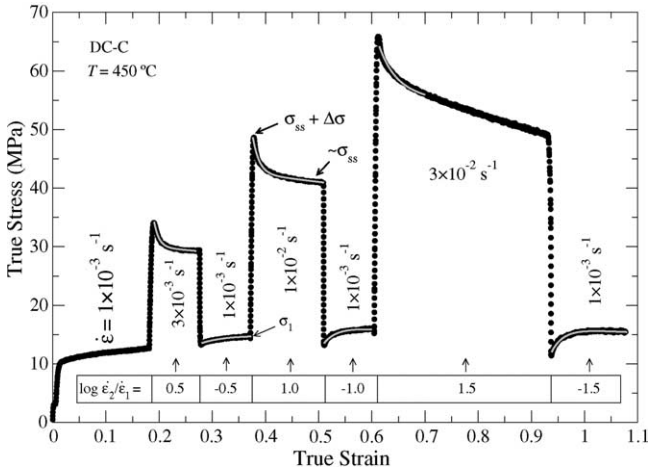

Fig. 1. Data are shown for a strain-rate-change test on AA5083 material DC-C at 450 °C. Fits to the stress transients following rate changes are shown.

[25]:

$$\sigma(\epsilon) = \sigma_{ss} + \Delta\sigma \exp\left(\frac{-\epsilon}{\epsilon_0}\right), \quad (3)$$

where $\sigma(\epsilon)$ is the transient true flow stress, ϵ is true strain following the rate change, $\Delta\sigma$ the size of the peak in transient stress immediately following the rate change, which is referenced to the steady-state flow stress σ_{ss} at the new rate, and ϵ_0 is a decay constant. For tests in which engineering strain rate is constant, as in the present study, the steady-state term can be multiplied by $\exp(-\epsilon/n)$ to account for the slight reduction in true-strain rate with increasing strain. In fitting Eq. (3) to experimental data, only three parameters are fit: σ_{ss}, $\Delta\sigma$, and ϵ_0. Fits of Eq. (3), shown in Fig. 1, describe the observed creep transients quite well. The parameters of Eq. (3) produced by fitting to data using a variety of strain-rate changes have been previously reported [25]. For these fits, the σ_{ss} values agreed closely with flow stress values measured for steady-state conditions at corresponding strain rates. This previous work, however, did not investigate the details of transient decay with strain.

A model was recently proposed for the general prediction of creep transient magnitudes, and this model is readily represented by a graphical construct [25]. Fig. 2 presents an extension of this graphical construct applied to SD creep transients produced (a) by strain-rate changes and (b) by stress changes. In this construct, the logarithm of the ratio of flow stresses is plotted against the logarithm of the ratio of strain rates. Values with a subscript of 1 indicate an initial steady-state condition, and values with a subscript of 2 indicate a new condition established from condition 1 by either a change in applied flow stress or applied true-strain rate. Steady-state data produce a straight line on this plot, with a slope equal to the strain-rate sensitivity, $m = 1/n$. Data taken using the peak of the creep transient immediately following a change from steady-state condition 1 to new condition 2, which is a constant-structure test, produce a transient line with a slope of m^*. The constant-structure assumption [12,13] indicates that mobile dislocation densities before and immediately after the change are identical, i.e. $\rho_1 = \rho_2$. For rate changes performed from a steady-state condition, ρ_1 is the established equilibrium mobile dislocation density for steady-state flow at rate $\dot{\epsilon}_1$. The angle between the steady-state and transient lines, θ, is a measure of the relative size of creep transients. The m and m^* values are observed to be invariant with temperature under conditions for which SD creep governs deformation [25]. For SRC tests, the transient line will decay toward the steady-state line in the manner shown by arrows in Fig. 2(a). For stress-change tests, the transient line will decay toward the steady-state line in the manner shown by arrows in Fig. 2(b).

Fig. 3(a) shows transient data, as reported in [25], immediately following strain-rate changes, i.e. $\epsilon = 0$, in the manner of Fig. 2(a). For each transient data point shown, an independent value of ϵ_0 was fit. Fig. 3(b) and (c) contain plots of transient data, not previously reported, at strains of $0.5\epsilon_0$ and $1.5\epsilon_0$, respectively. Fig. 3(b) and (c) reveals that the transient line decays toward the steady-state as strain increases. More importantly, it is shown that the transient data remain approximately linear as they decay with strain toward steady state. The linear fits to transient data in Fig. 3(b) and (c) produce fit correlation coef-

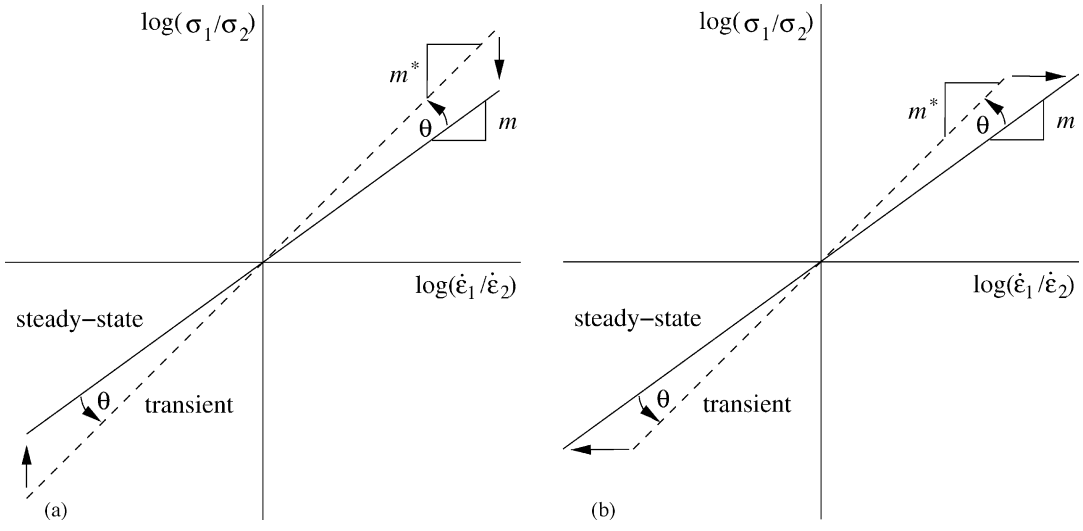

Fig. 2. Graphical constructs are shown to represent transient conditions for: (a) strain-rate-change tests and (b) stress-change tests under solute-drag creep.

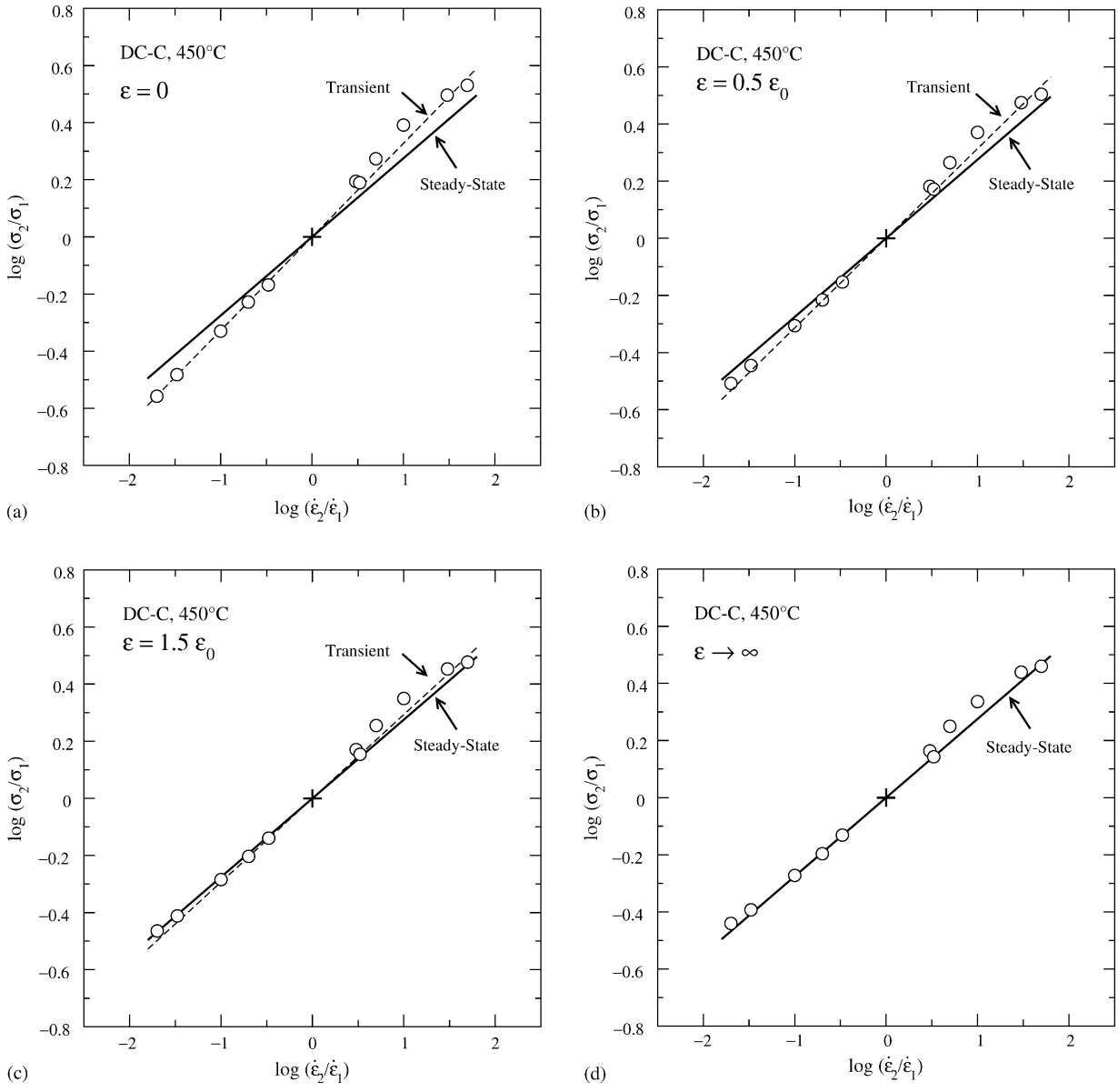

Fig. 3. The decay of stress transients with strain is demonstrated using the graphical construct for transient lines plotted at strains of: (a) $\epsilon = 0$, (b) $\epsilon = 0.5\epsilon_0$, (c) $\epsilon = 1.5\epsilon_0$, and (d) $\epsilon \to \infty$ following rate changes.

ficients ($R^2 = 0.998$) equivalent to that of the transient data in Fig. 3(a), indicating that the transient data truly remain linear, to within the experimental uncertainty, while decaying toward steady state. Fig. 3(d) shows the data upon reaching steady state, as reported in [25]. Material CC-A produces very similar results to those shown for material DC-C. Using the procedure shown in Fig. 3, the angle between the transient and steady-state lines, θ, was measured as a function of strain for materials DC-C and CC-A. These new measurements are presented in Fig. 4 as a plot of θ versus ϵ/ϵ_0, where $\epsilon_0 = 0.02$ is the average value calculated from all transient data. This figure clearly shows that θ decays exponentially with strain in the same manner as observed for the decay of stress transients (Eq. (3)). The transient and steady-state lines of Fig. 2 were found to be independent of temperature, and the values of ϵ_0 were not observed to change significantly with temperature [25].

Figs. 2 and 4 provide a means of predicting creep transients across all temperatures and rates for which SD creep dominates behavior. Consider the transient line of Figs. 2 and 3 to have a slope $m'(\epsilon)$, which varies with strain across the range $m^* \geq m' \geq m$. At the transient peak $m' = m^*$, and at steady state $m' = m$. The transient values, subscript of 2, after a change from a steady-state condition, subscript of 1, are then given by the following relation:

$$\log\left(\frac{\sigma_2}{\sigma_1}\right) = m' \log\left(\frac{\dot{\epsilon}_2}{\dot{\epsilon}_1}\right). \tag{4}$$

The geometry of Fig. 2 provides the following relationship for m' as a function of θ:

$$m' = \frac{m + \tan\theta}{1 - m\,\tan\theta}. \tag{5}$$

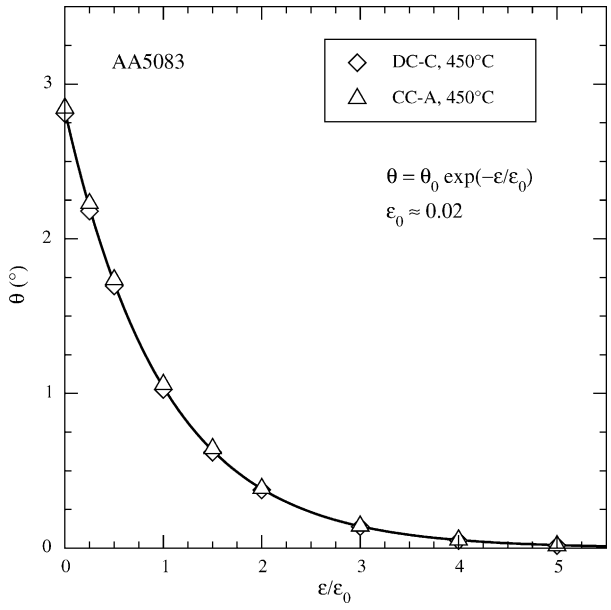

Fig. 4. The decay in the angle, θ, between the transient and steady-state lines with strain is shown.

Considering the values previously measured for θ at its maximum, immediately following the change from condition 1 to 2 [25], the following small-angle approximation produces a maximum error of less than 1%:

$$m' = \frac{m + \theta}{1 - m\theta}. \tag{6}$$

Applying the dependence of θ on strain observed in Fig. 4 produces the following relation:

$$m' = \frac{m + \theta_0 \exp(-\epsilon/\epsilon_0)}{1 - m\theta_0 \exp(-\epsilon/\epsilon_0)}. \tag{7}$$

The combination of Eqs. (4) and (7) provides a model for the general prediction of transients produced under SD creep by any change from a condition of steady-state deformation.

Data presented in the format of Fig. 2 provide a unique opportunity to probe the stress dependencies of ρ and $\bar{v}$ (Eq. (2)), quantities which are extremely difficult to measure by direct means. It can be shown from the Orowan relation (Eq. (2)) that, under constant-structure conditions,

$$\frac{\partial \ln \bar{v}}{\partial \ln \tau} = \left.\frac{\partial \ln \dot{\gamma}}{\partial \ln \tau}\right|_{\rho}. \tag{8}$$

Expressing the results of Figs. 2 and 3 in shear quantities produces the following relationship for the initial transient line:

$$\left.\frac{\partial \ln \dot{\gamma}}{\partial \ln \tau}\right|_{\rho} = \frac{1}{m^*}. \tag{9}$$

Equating the left side of Eq. (8) with the right side of Eq. (9) and integrating provides the dependence of dislocation glide velocity on stress under solute drag as

$$\bar{v} = B\tau^{1/m^*}, \tag{10}$$

where B is a constant at a given temperature. Thus, the transient line of Fig. 2 provides a measure for the dependence of dislocation glide velocity on stress under SD creep. Steady-state data, then, provide a means of measuring the dependence of equilibrium mobile dislocation density on stress. Because there is no grain-size dependence for SD creep, i.e. $p = 0$ [26], Eq. (1) can be simplified for a constant temperature to $\dot{\gamma} = K\tau^{1/m}$, as written in terms of shear quantities. Combining this simplified form of Eq. (1) with Eqs. (10) and (2) yields the following relation for steady-state deformation:

$$\left.\frac{\partial \ln \rho}{\partial \ln \tau}\right|_{ss} = \frac{1}{m} - \frac{1}{m^*}. \tag{11}$$

Thus, the dependence of mobile dislocation density on flow stress at steady state is

$$\rho = C\tau^{1/m - 1/m^*}, \tag{12}$$

where C is a constant at a given temperature. Thus, dislocation glide velocity depends on applied stress to the $1/m^*$ power, and equilibrium mobile dislocation density depends on stress to the $1/m - 1/m^*$ power. Data shown in Table 2 clearly indicate that the increase in n beyond three observed for commercial Al–Mg alloys is primarily associated with a significant increase in the stress dependence of dislocation glide velocity $1/m^*$. The stress dependence of equilibrium mobile dislocation density $1/m - 1/m^*$ is only slightly changed in AA5083 from that of the low-impurity, binary Al–Mg material studied by Mills et al.

Table 2
Steady-state and transient creep data

Material	m	m^*	$\frac{1}{m^*}$	$\frac{1}{m} - \frac{1}{m^*}$
Al–5.5 at.% Mg[a]	0.32	0.48	2.1	1.0
AA5083	0.27	0.32	3.1	0.6

[a] Data from Mills et al. [12].

4. Conclusions

An analysis of creep transients for solute-drag creep in AA5083 materials has revealed the following:

(1) A recently proposed model, readily represented in a simple graphical construct, can be used to analyze creep transients and their decay with strain.
(2) The graphical construct represents steady-state data with a line of slope m and transient data as a line of initial slope m^*.
(3) Transient data remain linear when plotted in this manner as they decay with strain toward the steady-state line.
(4) The angle between the transient line and the steady-state line, θ, decays exponentially with strain and observes the same decay constant, ϵ_0, as the average of individual creep transients.
(5) A model is proposed to predict creep transients produced under SD creep by any general change from a condition of steady-state deformation.
(6) The dislocation glide velocity is proportional to stress to the $1/m^*$ power, and the mobile dislocation density at steady

state is proportional to stress raised to the $1/m - 1/m^*$ power under SD creep.

(7) The high stress exponent of commercial 5000-series materials, relative to low-impurity Al–Mg materials, is primarily because of an increased dependence of dislocation glide velocity on stress.

Acknowledgment

The authors gratefully acknowledge support from the General Motors Corp. for this work.

References

[1] O.D. Sherby, R.A. Anderson, J.E. Dorn, Trans. AIME (1951) 643–652.
[2] W.R. Cannon, O.D. Sherby, Metall. Trans. A 1 (1970) 1030–1032.
[3] R. Horiuchi, M. Otsuka, Trans. Jpn. Inst. Met. 13 (1972) 284–293.
[4] K.L. Murty, F.A. Mohamed, J.E. Dorn, Acta Metall. 20 (1972) 1009–1018.
[5] F.A. Mohamed, T.G. Langdon, Acta Metall. 22 (1974) 779–788.
[6] H. Oikawa, J. Kariya, S. Karashima, Met. Sci. 8 (1974) 106–111.
[7] H. Oikawa, N. Matsuno, S. Karashima, Met. Sci. 9 (1975) 209–212.
[8] H. Oikawa, K. Sugawara, S. Karashima, Trans. Jpn. Inst. Met. 19 (1978) 611–616.
[9] F.A. Mohamed, Scripta Metall. 12 (1978) 99–102.
[10] P. Yavari, F.A. Mohamed, T.G. Langdon, Acta Metall. 29 (1981) 1495–1507.
[11] P. Yavari, T.G. Langdon, Acta Metall. 30 (1982) 2181–2196.
[12] M.J. Mills, J.C. Gibeling, W.D. Nix, Acta Metall. 33 (1985) 1503–1514.
[13] M.J. Mills, J.C. Gibeling, W.D. Nix, Acta Metall. 34 (1986) 915–925.
[14] V. Raman, T.G. Langdon, Acta Metall. 37 (1989) 725–737.
[15] T.R. McNelley, D.J. Michel, A. Salama, Scripta Metall. 23 (1989) 1657–1662.
[16] H.J. McQueen, M.E. Kassner, in: T.R. McNelley, H.C. Heikkenen (Eds.), Superplasticity in Aerospace II, The Minerals, Metals and Materials Society, Warrendale, PA, 1990, pp. 189–206.
[17] M.E. Kassner, N.Q. Nguyen, G.A. Henshall, H.J. McQueen, Mater. Sci. Eng. A 132 (1991) 97–105.
[18] G.A. Henshall, M.E. Kassner, H.J. McQueen, Metall. Trans. A 23 (1992) 881–889.
[19] E.M. Taleff, D.R. Lesuer, J. Wadsworth, Metall. Mater. Trans. A 27 (1996) 343–352.
[20] T. Ito, S. Shibasaki, M. Koma, M. Otsuka, J. Jpn. Inst. Met. 66 (2002) 409–417.
[21] T. Ito, M. Koma, S. Shibasaki, M. Otsuka, J. Jpn. Inst. Met. 66 (2002) 476–484.
[22] M.-A. Kulas, P.E. Krajewski, T.R. McNelley, E.M. Taleff, in: Z. Jin, A. Beaudoin, T. Bieler, B. Radhakrishnan (Eds.), Hot Deformation of Aluminum Alloys III, TMS, Warrendale, PA, 2003, pp. 499–507.
[23] E.M. Taleff, in: E.M. Taleff, in: P.A. Friedman, P.E. Krajewski, R.S. Mishra, J.G. Schroth (Eds.), Advances in Superplasticity and Superplastic Forming, TMS, Warrendale, PA, 2004, pp. 85–94.
[24] M.-A. Kulas, W.P. Green, E.C. Pettengill, P.E. Krajewski, E.M. Taleff, in: E.M. Taleff, P.A. Friedman, P.E. Krajewski, R.S. Mishra, J.G. Schroth (Eds.), Advances in Superplasticity and Superplastic Forming, TMS, Warrendale, PA, 2004, pp. 127–138.
[25] M.-A. Kulas, W.P. Green, E.M. Taleff, P.E. Krajewski, T.R. McNelley, Metall. Mater. Trans. A 36 (2005) 1249–1261.
[26] E.M. Taleff, G.A. Henshall, T.G. Nieh, D.R. Lesuer, J. Wadsworth, Metall. Mater. Trans. A 29 (1998) 1081–1091.
[27] O.D. Sherby, P.M. Burke, Prog. Mater. Sci. 13 (1968) 325–390.
[28] J.G. Schroth, in: E.M. Taleff, P.A. Friedman, P.E. Krajewski, R.S. Mishra, J.G. Schroth (Eds.), Advances in Superplasticity and Superplastic Forming, TMS, Warrendale, PA, 2004, pp. 9–20.
[29] E.M. Taleff, P.J. Nevland, P.E. Krajewski, Metall. Mater. Trans. A 32 (2001) 1119–1130.
[30] T.G. Langdon, Metall. Trans. A 13 (1982) 689–701.
[31] A. Arieli, A.K. Mukherjee, Metall. Trans. A 13 (1982) 717–732.
[32] O.D. Sherby, J. Wadsworth, Mater. Sci. Technol. 1 (1985) 925–936.
[33] O.D. Sherby, J. Wadsworth, Prog. Mater. Sci. 33 (1989) 169–221.
[34] T.G. Langdon, Mater. Sci. Eng. A 137 (1991) 1–11.
[35] R.W. Evans, B. Wilshire, Creep of Metals and Alloys, Institute of Metals, London, 1985.
[36] R.W. Evans, B. Wilshire, Introduction to Creep, Institute of Metals, London, 1993.
[37] B. Wilshire, Metall. Mater. Trans. A 33 (2002) 241–248.
[38] H. Burt, B. Wilshire, Metall. Mater. Trans. A 35 (2004) 1691–1701.
[39] J. Weertman, J. Appl. Phys. 28 (1957) 1185–1189.
[40] J. Weertman, Trans. Metall. Soc. AIME 218 (1960) 207–218.
[41] E.M. Taleff, J. Qiao, in: T. Srivatsan, D.R. Lesuer (Eds.), Modeling the Performance of Engineering Structural Materials II, TMS, Warrendale, PA, 2001, pp. 3–12.
[42] A.H. Cottrell, M.A. Jaswon, Proc. Roy. Soc. A 199 (1949) 104–114.
[43] S. Takeuchi, A.S. Argon, Phil. Mag. A 40 (1979) 65–75.
[44] R. Fuentes-Samaniego, R. Gasca-Neri, J.P. Hirth, Phil. Mag. A 49 (1984) 31–43.
[45] R. Fuentes-Samaniego, J.P. Hirth, Phys. Stat. Sol. B 121 (1984) 101–109.
[46] W.L. James, Ph.D. Thesis, Stanford University, Stanford, CA, 1986.
[47] W.L. James, D.M. Barnett, in: S. Saimoto, G.R. Purdy, G.V. Kidson (Eds.), Solute–Defect Interaction Theory and Experiment, Pergamon Press, 1986.